

## Novel Tools and Methods

# MEYE: Web App for Translational and Real-Time Pupillometry

 Raffaele Mazziotti,<sup>1,2,\*</sup> Fabio Carrara,<sup>5,\*</sup> Aurelia Viglione,<sup>2,4</sup> Leonardo Lupori,<sup>3</sup> Luca Lo Verde,<sup>2</sup> Alessandro Benedetto,<sup>6</sup> Giulia Ricci,<sup>1</sup> Giulia Sagona,<sup>2,3</sup> Giuseppe Amato,<sup>5</sup> and Tommaso Pizzorusso<sup>1,2,4</sup>

<https://doi.org/10.1523/ENEURO.0122-21.2021>

<sup>1</sup>Department of Neuroscience, Psychology, Drug Research and Child Health (NEUROFARBA), University of Florence, 50135 Florence, Italy, <sup>2</sup>Institute of Neuroscience, National Research Council, 1-56124 Pisa, Italy, <sup>3</sup>Department of Developmental Neuroscience, IRCCS Stella Maris Foundation, 56128 Pisa, Italy, <sup>4</sup>Laboratory of Biology BIO@SNS, Scuola Normale Superiore, 1-56124 Pisa, Italy, <sup>5</sup>Istituto di Scienza e Tecnologia dell'Informazione (ISTI), 1-56124 Pisa, Italy, and <sup>6</sup>Department of Translational Research on New Technologies in Medicine and Surgery, University of Pisa, 56127 Pisa, Italy

## Abstract

Pupil dynamics alterations have been found in patients affected by a variety of neuropsychiatric conditions, including autism. Studies in mouse models have used pupillometry for phenotypic assessment and as a proxy for arousal. Both in mice and humans, pupillometry is noninvasive and allows for longitudinal experiments supporting temporal specificity; however, its measure requires dedicated setups. Here, we introduce a convolutional neural network that performs online pupillometry in both mice and humans in a web app format. This solution dramatically simplifies the usage of the tool for the nonspecialist and nontechnical operators. Because a modern web browser is the only software requirement, this choice is of great interest given its easy deployment and setup time reduction. The tested model performances indicate that the tool is sensitive enough to detect both locomotor-induced and stimulus-evoked pupillary changes, and its output is comparable to state-of-the-art commercial devices.

*Key words:* arousal; neural network; oddball; pupillometry; virtual reality; web app

## Significance Statement

Alteration of pupil dynamics is an important biomarker that can be measured noninvasively and across different species. Although pupil size is driven primarily by light, it can also monitor arousal states and cognitive processes. Here we show an open-source web app that, through deep learning, can perform real-time pupil size measurements in both humans and mice, with accuracy similar to commercial-grade eye trackers. The tool requires no installation, and pupil images can be captured using infrared webcams, opening the possibility of performing pupillometry widely, cost-effectively, and in a high-throughput manner.

## Introduction

Pupillometry, the measurement of pupil size fluctuations over time, provides useful insights into clinical settings and basic research activity. Light level is the primary determinant of pupil size, although non-light-driven pupil fluctuations, widely assumed as an indicator of arousal through locus coeruleus activity, can be used to index brain state across species (McGinley et al., 2015; Lee and

Margolis, 2016; Reimer et al., 2016). Higher cognitive and emotional processes are also able to evoke tonic or phasic pupillary changes, such as attention (Binda et al., 2013a), memory load (Wierda et al., 2012), novelty (Angulo-Chavira et al., 2017; Krebs et al., 2018; Montes-Lourido et al., 2021), pain (Connelly et al., 2014; Azevedo-Santos and DeSantana, 2018; Charier et al., 2019), and more general cortical sensory

Received March 24, 2021; accepted June 9, 2021; First published September 13, 2021.

The authors declare no competing financial interests.

Author contributions: R.M., F.C., G.A., and T.P. designed research; R.M., F.C., A.V., L.L., L.L.V., A.B., G.R., and G.S. performed research; R.M., F.C., L.L., L.L.V., and A.B. analyzed data; R.M., F.C., A.B., G.A., and T.P. wrote the paper.

processing (Binda et al., 2013b; Lee and Margolis, 2016) in humans and in animal models.

A growing body of work shows how pupillometry can be used as a possible biomarker for numerous neurologic and psychiatric conditions in early development and adult subjects (Aleman et al., 2004; Blaser et al., 2014; Rorick-Kehn et al., 2014; Frost et al., 2017; Nyström et al., 2018; Chougule et al., 2019; Gajardo et al., 2019; Oh et al., 2019, 2020; Artoni et al., 2020; Burley and van Goozen, 2020; Iadanza et al., 2020; Obinata et al., 2020; Winston et al., 2020; El Ahmadieh et al., 2021). Spontaneous and voluntary modulation of pupil fluctuations has also been used to facilitate human–computer interaction in normal subjects (Mathôt et al., 2016; Beggiano et al., 2018; Ponzio et al., 2019) and patients with severe motor disabilities. For example, pupil dynamics is used to assess communication capability in locked-in syndrome, a crucial factor for the determination of a minimally conscious state (Olivia et al., 2013; Stoll et al., 2013). Pupillometry is also becoming a valuable tool for child neurology, to facilitate risk assessment in infants. For example, the pupil light reflex (PLR) during infancy seems to predict the later diagnosis and severity of autism spectrum disorders (ASDs; Nyström et al., 2018). Intriguingly, pupil alterations are also present in several ASD mouse models (Artoni et al., 2020).

Pupillometry has several advantages compared with other physiological methods: it is noninvasive and can be performed by nonspecialized personnel on noncollaborative and preverbal subjects (like infants), allowing the design of longitudinal experiments to permit temporal specificity. More importantly, it can be conducted similarly across different species from mice to humans, guaranteeing maximal translatability of the protocols and results (Aleman et al., 2004; Rorick-Kehn et al., 2014; Artoni et al., 2020). Given these assumptions, it is vital to introduce a simple, versatile tool used in a range of settings, from the laboratory to the clinical or even domestic environment. Available open-source methods require complicated steps for the installation and configuration of custom software not suitable for nontechnical operators. Moreover, these tools were tested exclusively in one species

This work was partially supported by Horizon 2020 projects AI4EU (under GA Grant 825619) and AI4Media (under GA Grant 951911); funding from the Italian Ministry for university and research Grant MIUR-PRIN 2017HMH8FA; Associazione Italiana per la sindrome di Rett Project (AIRETT) “Validation of Pupillometry as a Biomarker for Rett Syndrome and Related Disorders: Longitudinal Assessment and Relationship with Disease”; Orphan Disease Center University of Pennsylvania Grant MDBR-19-103-CDKL5; and Associazione “CDKL5 - Insieme verso la cura.”

\*R.M. and F.C. contributed equally to this work.

We thank NVIDIA for donation of the Jetson AGX Xavier Developer Kit. We also thank Dr. Viviana Marchi, Dr. Grazia Rutigliano, and Dr. Carlo Campagnoli for critical reading of the manuscript.

Correspondence should be addressed to Raffaele Mazziotti at [raffaele.mazziotti@in.cnr.it](mailto:raffaele.mazziotti@in.cnr.it).

<https://doi.org/10.1523/ENEURO.0122-21.2021>

Copyright © 2021 Mazziotti et al.

This is an open-access article distributed under the terms of the Creative Commons Attribution 4.0 International license, which permits unrestricted use, distribution and reproduction in any medium provided that the original work is properly attributed.

[mice (Privitera et al., 2020), humans (Yiu et al., 2019)], and none of them were applied in cognitive experiments that usually involve small pupil changes associated with high variability.

In this work, we have developed a deep learning tool called MEYE, using convolutional neural networks (CNNs) to detect and measure real-time changes in pupil size both in humans and mice in different experimental conditions. Furthermore, the MEYE web app, performs pupil area quantification and blink detection, all within a single network. By embedding artificial intelligence algorithms in a web browser to process real-time webcam streams or videos of the eye, MEYE can be used by nontechnical operators, opening the possibility to perform pupillometry widely, cost-effectively, and in a high-throughput manner. This architecture is resistant to different illumination conditions, allowing the design of basic neuroscience experiments in various experimental settings, such as behavior coupled with electrophysiology or imaging such as two-photon microscopy. To describe the performance of the MEYE web app in different settings, we tested the app in both mice and humans. In mice, we recorded both running speed and pupil size during visual and auditory stimulation (AS). In humans, we tested MEYE capabilities to detect the PLR. Furthermore, we performed a visual odd-ball paradigm (Liao et al., 2016; Aggius-Vella et al., 2020; LoTempio et al., 2021), comparing pupil size and eye position measurements obtained from MEYE with one of the most used commercial eye-tracker systems: the EyeLink 1000. Finally, we released a dataset of 11,897 eye images that can be used to train other artificial intelligence tools.

## Materials and Methods

### Datasets

For this study, we collected a dataset (Fig. 1A) composed of 11,897 grayscale images of human (4285) and mouse (7612) eyes. The majority of the pictures are of mouse eyes during head fixation sessions (5061 sessions) in a dark environment using infrared (IR; 850 nm) light sources. In this environment, the pupil is darker than the rest of the image. We also collected mouse eyes [two-photon imaging mice (2P mice), 2551] during two-photon  $\text{Ca}^{2+}$  imaging. In this particular condition, the pupil is inverted in color and tends to be brighter than the iris. Finally, we acquired images of human eyes in IR light (4285 eyes) during virtual reality (VR) experiments (wearing a headset for virtual reality), using an endoscopic camera ([www.misumi.com.tw/](http://www.misumi.com.tw/)). The dataset contains 1596 eye blinks, 841 images in the mouse, and 755 photographs in the human datasets. Five human raters segmented the pupil in all pictures (one per image), using custom labeling scripts implemented in MATLAB or Python by manual placement of an ellipse or polygon over the pupil area. Raters flagged blinks using the same code.

### CNN architecture

The CNN model (Fig. 1C) takes  $128 \times 128$  grayscale images as input and produces the following three outputs:

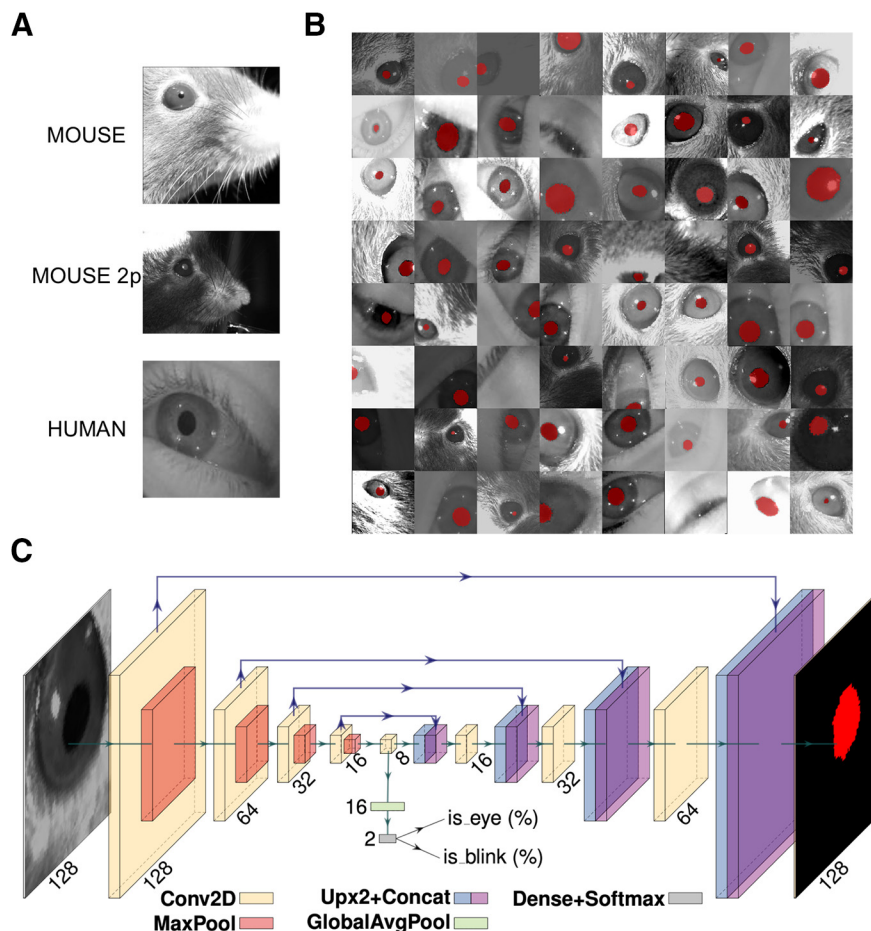


**Figure 1.** Dataset, CNN architecture, and performances. **A**, Examples of images taken from the dataset. The first image depicts a head-fixed mouse with dark pupils, the second one is a head-fixed mouse with a bright pupil, during two-photon microscope sessions. The last image is a human eye taken during experiments wearing virtual reality goggles. **B**, The 64 examples of data augmentation fed to CNN. The images are randomly rotated, cropped, flipped (horizontally or vertically), and changed in brightness/contrast/sharpness. **C**, CNN architecture with an encoder–decoder “hourglass” shape. The encoder part comprises a sequence of convolutional layers. Starting from the last encoder output, the decoder part iteratively upsamples and fuses feature maps with corresponding encoder maps to produce the output pixel map. The pixel probability map and eye/blink probabilities are computed by applying the sigmoid activation to the network outputs in an element-wise manner.

(1) a  $128 \times 128$  probability map of each pixel belonging to the pupil; (2) the probability the image contains an eye; and (3) the probability the image depicts a blinking eye. We evaluated three architectures: two were based on DeepLabv3+ (Chen et al., 2018), a family of image segmentation models that use atrous convolutions and spatial pyramid pooling, which are known to improve robustness to scale changes. The two models differ for the CNN backbone adopted, respectively, ResNet-50 (He et al., 2016) and MobileNet V3 (Howard et al., 2019) CNNs. The third evaluated model is a specialized variant of the U-Net architecture (Ronneberger et al., 2015), a widely used CNN in image segmentation tasks. The model has an encoder–decoder “hourglass” architecture; the encoder part comprises a sequence of convolutional layers with ReLU activation and  $2 \times 2$  maximum pooling operation, each halving the spatial resolution of feature maps at every layer; this produces a sequence of feature maps of diminishing spatial dimensions that

provides both spatially local information and global context for the subsequent steps. Starting from the last encoder output, the decoder part iteratively upsamples and fuses feature maps with corresponding encoder maps, using convolutional layers, to produce the output pixel map. All convolutional layers have  $16 \times 3 \times 3$  kernels and pad their input to obtain output of the same shape. Convolutional layer upsampling and downsampling were changed by a factor of 2 (Fig. 1C). In all the tested architectures, eye and blink probabilities are predicted by an additional branch that applies global average pooling and a two-output fully connected layer to the bottleneck feature map. The pixel probability map and eye/blink probabilities are computed by applying the sigmoid activation to the network outputs element wise. Among the tested architectures, we chose to adopt the UNet variant in this work, as we observed it provided the best tradeoff in terms of speed and segmentation quality (for further

information see: <https://github.com/fabiocarrara/meve/wiki/MEYE-Models>).

### Augmentation, training, and validation

We randomly split the dataset into training, validation, and test subsets following a 70%/20%/10% split. We performed strong data augmentation during the training phase by applying random rotation, random cropping, random horizontal and vertical flipping, and random brightness/contrast/sharpness changes; images were resized to  $128 \times 128$  before feeding them to the CNN (Fig. 1B).

For validation and test images, we used a  $128 \times 128$  crop centered on the pupil. We computed the binary cross-entropy for all outputs (pixels and eye/blink logits) and took the sum as the loss function to minimize. The network was trained with the AdaBelief optimizer (Zhuang et al., 2020) for 750 epochs with a learning rate of 0.001. The best performing snapshot on the validation set was selected and evaluated on the test set.

### MEYE: web browser tool

We built a web app for pupillometry on recorded or live-captured videos harnessing a CNN segmentation model as the core component. The trained models have been converted to a web-friendly format using *TensorFlow.js*, thus enabling predictions on the user machine using a web browser.

This choice greatly facilitates the deployment and reduces setup time, as a modern web browser is the only minimum requirement. Once loaded, an Internet connection is not mandatory, as no data leaves the user's browser, and all the processing is performed on the user's machine. This implies that performance greatly depends on the user's hardware; if available, hardware (graphics processing unit (GPU)) acceleration is exploited automatically by *TensorFlow.js*. In our tests, a modern laptop shipping an Intel(R) Core(TM) i7-9750H 2.60 GHz CPU and an Intel(R) UHD Graphics 630 GPU can process up to 28 frames/s (fps).

The web app also offers additional features that facilitate the recording process, such as the following: processing of prerecorded videos or real-time video streams captured via webcam; ROI placement via user-friendly web user interface (UI; drag and drop) and automatic repositioning following tracked pupil center; embedded tunable preprocessing (image contrast/brightness/gamma adjustment and color inversion) and postprocessing (map thresholding and refinement via mathematical morphology); support for registering trigger events; live plotting of pupil area and blink probability; and data export in CSV format including pupil area, blink probability, eye position, and trigger channels.

### Behavioral experiments on mice

#### Animal handling

Mice were housed in a controlled environment at 22°C with a standard 12 h light/dark cycle. During the light phase, a constant illumination <40 lux from fluore-

scent lamps was maintained. Food (standard diet, 4RF25 GLP Certificate, Mucedola) and water were available *ad libitum* and were changed weekly. Open-top cages ( $36.5 \times 20.7 \times 14$  cm;  $26.7 \times 20.7 \times 14$  cm for up to five adult mice; or  $42.5 \times 26.6 \times 15.5$  cm for up to eight adult mice) with wooden dust-free bedding were used. All the experiments were conducted following the directives of the European Community Council and approved by the Italian Ministry of Health (1225/2020-PR). All necessary efforts were made to minimize both stress and the number of animals used. The subjects used in this work were three female 3-month-old C57BL/6J mice for the auditory stimulation and five male 2-month-old mice for the VR experiment.

#### Surgery

The mouse was deeply anesthetized using isoflurane (3% induction, 1.5% maintenance). Then it was mounted on a stereotaxic frame through the use of ear bars. Prilocaine was used as a local anesthetic for the acoustic meatus. The eyes were treated with a dexamethasone-based ophthalmic ointment (Tobradex, Alcon Novartis) to prevent cataract formation and keep the cornea moist. Body temperature was maintained at 37°C using a heating pad monitored by a rectal probe. Respiration rate and response to toe pinch were checked periodically to maintain an optimal level of anesthesia. Subcutaneous injection of lidocaine (2%) was performed before scalp removal. The skull surface was carefully cleaned and dried, and a thin layer of cyanoacrylate was poured over the exposed skull to attach a custom-made head post that was composed of a 3D-printed base equipped with a glued set screw (12 mm long, M4 thread; catalog #SS4MS12, Thorlabs). The implant was secured to the skull using cyanoacrylate and UV curing dental cement (Fill Dent, Bludental). At the end of the surgical procedure, the mice recovered in a heated cage. After 1 h, mice were returned to their home cage. Paracetamol was used in the water as antalgic therapy for 3 d. We waited 7 d before performing head-fixed pupillometry to provide sufficient time for the animal to recover.

#### Head fixation

In the awake mouse head fixation experiments, we used a modified version of the apparatus proposed by Silasi et al. (2016), equipped with a 3D-printed circular treadmill (diameter, 18 cm). Components are listed in Table 1. A locking ball socket mount (TRB1/M) was secured to an aluminum breadboard (MB2020/M) using two optical posts (TR150/M-P5) and a right-angle clamp (RA90/M-P5). The circular treadmill was blocked between the base plate pillar rod and the optical post through a ball-bearing element (BU4041, BESZY) to allow the spinning of the disk with low effort. To couple the head-fixing thread on the mouse to the locking ball, an ER025 post was modified by retapping one end of it with M4 threads to fit the ball and socket mount. Velocity was detected using an optical mouse under the circular treadmill. Pupillometry was performed using a USB camera (oCam-5CRO-U, Withrobot) equipped with a 25 mm M12 lens connected to a Jetson AGX Xavier Developer Kit (NVIDIA)

**Table 1: Head fixation apparatus components (thorlabs.com)**

Part number	Description	Quantity	Price (€)
TRB1/M	Locking ball and socket mount M4	1	55.83
TR150/M-P5	Optical post M4–M6, 150 mm, 5 pack	1	29.97
RA90/M-P5	Right-angle clamp	1	45.7
MB2020/M	Aluminum breadboard	1	72.3
RS075P/M	Pedestal pillar post	1	21.63
SS4MS12	Set screws 12 mm long, M4	1	5.61
AP4M3M	Adaptor M4–M3	5	1.91
ER025	Cage assembly rod	5	4.73
SS6MS12	Set screws 12 mm long, M6	1	5.55
CF038C-P5	Clamping fork	1	46.49
Total			289.72

running a custom Python3 script (30 fps). The Jetson hardware was connected with an Arduino UNO microcontroller board through GPIO (general purpose input/output) digital connection. The Arduino UNO managed the auditory stimuli through a speaker (3 inch; model W3-1364SA, Tang Band Speaker).

### Behavioral procedures

Mice were handled for 5 min each day during the week preceding the experiments; then, they were introduced gradually to head fixation for an increasing amount of time for 5 d. During days 1 and 2, we performed two sessions of 10 min of head fixation, one in the morning and one in the afternoon. On day 3, we performed one session of 20 min; on day 4, 30 min; and on day 5, 35 min. Each recording started with 5 min of habituation. We exposed the animal to auditory stimuli during the last day. During each head fixation session, a curved monitor (24 inches; model CF390, Samsung) was placed in front of the animal (distance, 13 cm) showing a uniform gray with a mean luminance of 8.5 cd/m<sup>2</sup>. The frequency of tone 1 was 3000 Hz, and of tone 2, 4000 Hz, both at 70 dB, a duration of 20 s, and an interstimulus interval of 120 s. Virtual reality was composed of a  $\gamma$ -linearized procedural virtual corridor with episodic visual stimulation written in C# and Unity. The virtual corridor was composed of sine-wave gratings at different orientations (wall at 0°; floor at 90°), and spatial frequencies (from 0.06 to 0.1 cycles/°). The position of the animal in the virtual corridor was updated using an optical mouse connected to the circular treadmill. The episodic visual stimulus consisted of a square wave grating patch of 55° (in width and height) of visual space in the binocular portion of the visual field. The grating parameters were as follows: luminance, 8.5 cd/m<sup>2</sup>; orientation, 0°; contrast, 90%; spatial frequency, 0.1 cycles/°; drifting, 0.5 cycle/s.

### Data analysis

Data has been analyzed using Python 3. All tracks were loaded, and blink removal was applied using the blink detector embedded in MEYE. Blink epochs were filled using linear interpolation and median filtering (0.5 s). Spearman  $\rho$  rank-order correlation was performed using the function *corr* from Python library *pingouin* (Vallat, 2018). The z-score was obtained for each trial using the formula  $z = (X - \bar{X}_{\text{baseline}}) / S_{\text{baseline}}$ , where  $\bar{X}_{\text{baseline}}$  and  $S_{\text{baseline}}$  were respectively the average and the SD of the baseline.

To evaluate whether event-related transients (ERTs) amplitude was significantly different from baseline, a two-way repeated-measures ANOVA was computed on each time sample using the *pingouin* function *rm\_anova*. *Post hoc* analyses and multiple-comparison *p* value correction were conducted using the function *pairwise\_t* tests from *pingouin*. For both pupil size and velocity, we compared each time sample after sensory stimulation with the average value of the baseline, adjusting the *p* values using Benjamini–Hochberg FDR correction. For the behavioral state analysis, locomotion activity was identified using a threshold algorithm. We tagged as moving all the samples in which velocity was  $\geq 10\%$  with respect to the maximal speed of the animal. Paired *t* tests between behavioral states were performed using the function *t* test from *pingouin*. Comparison of eyes movements was conducted normalizing (range between  $-1$  and  $1$ ) data from both setups, upsampling MEYE data from 15 to 1000 fps using linear interpolation, and then calculating the mean absolute error (MAE), which was performed using the Python function *mean\_absolute\_error* from the library *sklearn*.

### Behavioral experiments on humans

#### PLR

Pupillometry has been performed using a MacBook Pro (Retina, 13 inch, Early 2015, Intel Core i5 dual-core 2.7 GHz, 8GB of RAM, Intel Iris Graphics 6100 card, 1536 MB) running the MEYE application on Firefox (84.0). The tool is able to compute online pupil size quantification, plotting the instantaneous pupil area and saving the results on file. Furthermore, the tool accepts four independent manual push-button triggers (keys “T” or “Y” on the keyboard). This feature allowed us to annotate stimulation events. A USB IR webcam (model Walfront5k3psmv97x, Walfront) equipped with a Varifocal 6–22 mm M12 objective (catalog #149129, Sodial) was used to acquire images of the eye. The camera was equipped with six IR LEDs to illuminate the eye uniformly, optimizing contrast between the iris and the pupil. Photic stimulation was delivered using an Arduino Due (Arduino) microcontroller connected via USB to the notebook and programmed to emulate a keyboard. The Arduino emulates a keyboard (using the *keyboard.h* library) to send event triggers to MEYE in the form of keystroke events. The microcontroller drives a stripe of four LEDs (WS2813, WorldSemi) using the

**FastLED.** *h* library, flashing bright white light for 500 ms with an interstimulus interval of 5 s (see Fig. 3A). The subject sat in front of a monitor screen (24 inches; model CF390, Samsung) at a distance of 60 cm, with the head stabilized by a chin rest and instructed to maintain fixation on a small dot presented in the center of the screen for the whole duration of the recording (57 s). A total of 10 flash stimuli have been presented through the strip of LEDs mounted above the screen.

#### Oddball paradigm corecordings

To compare the performances shown by the CNN system with that of a state-of-the-art commercial software, we coregistered pupillometry using MEYE and an EyeLink 1000 system, while nine participants (three males, six females; average age, 28.78 years) executed an oddball paradigm. The experiment was conducted in a quiet, dark room. The participant sat in front of a monitor screen (88 × 50 cm) at a distance of 100 cm, with their head stabilized by a chin rest. The viewing was binocular. Stimuli were generated with the PsychoPhysics Toolbox routines (Brainard, 1997; Pelli, 1997) for MATLAB (MATLAB r2010a, MathWorks) and presented on a  $\gamma$ -calibrated PROPixx DLP LED projector (VPixx Technologies) with a resolution of 1920 × 1080 pixels, and a refresh rate of 120 Hz. Pupil diameter was monitored at 1 kHz with an EyeLink 1000 system (SR Research) with an infrared camera mounted below the screen and recording from the right eye. The participant was instructed to maintain fixation on a small dot (0.5°) presented in the center of the screen for the whole duration of the recording (300 s). In this study, the visual stimuli consisted of the appearance of a high-probability stimulus (80% of times) defined as “Standard” and a lower probability stimulus (20% of times) defined as “Target.” The Standard stimulus consisted of a 100% contrast-modulated annular grating (mean luminance, 25 cd/m<sup>2</sup>), horizontally oriented, with a spatial frequency of 0.5 cpd, and with inner and outer diameters of 1.5° and 5°, respectively. The edges of the annulus were smoothed by convolving the stimulus with a Gaussian mask ( $\sigma = 0.5^\circ$ ). The Target stimulus had the same parameters as the Standard stimulus except that the orientation that was 45° (see Fig. 4A). The presentation duration of each trial, either the Standard (0°) or Target (45°) trial, was 200 ms with an inter-trial interval between two consecutive trials of 2800 ms. The phases of both the Target and the Standard stimuli were randomized across trials. The participants were instructed to press a button for a Target stimulus and not to respond for a Standard stimulus. The z-scored ERTs were computed as described for mice. The correlation was performed by taking the amplitude of the peaks of the Targets for each subject using both EyeLink and MEYE, and then performing the Spearman  $\rho$  rank-order correlation between the two measures.

#### Eye movement corecordings

For eye-tracking recording, we used both the MEYE tool and EyeLink 1000, as described above. In the smooth pursuit condition, a small dot (0.5°) moved on the screen horizontally, changing direction every 20° of the visual

field with a constant velocity of 8°/s. In the saccades condition, every 2.5 s the small dot abruptly changes position horizontally with a span of 20°.

#### Offline video analysis

The MP4 videos were loaded into MEYE, and the parameters were chosen by visually inspecting the quality of the pupillometry. Threshold values were 0.25, 0.15, and 0.5, with morphology FALSE, TRUE, TRUE for “human,” “mouse,” and “2P-mouse” videos respectively. Once the video analysis was completed, the CSV file was loaded into Python. Blink removal and linear interpolation were applied, then the track was plotted using the Python library *matplotlib*.

#### Data availability

The code and web app are freely available on Github: [github.com/fabiocarrara/meye](https://github.com/fabiocarrara/meye). MEYE is available at: [www.pupillometry.it](http://www.pupillometry.it). MEYE wiki is available at: <https://github.com/fabiocarrara/meye/wiki>. The dataset is available on: <https://doi.org/10.5281/zenodo.4488164>.

## Results

### Pupillometry in head-fixed mice

We tested our CNN-based pupillometer in two behavioral experiments involving locomotion-induced and stimulus-evoked pupillary changes. Pupil size was simultaneously recorded with running speed from head-fixed mice free to run on a circular treadmill (Fig. 2A). We used two different stimulation protocols: AS, and visual stimulation while the animal is freely exploring VR. The VR experiment included an initial period of habituation in which the animal navigated inside a virtual corridor for 5 min. After this period, a square visual stimulus was presented in the binocular portion of the visual field (duration, 20 s; interstimulus interval, 120 s, 10 times; Fig. 3A,B). The AS experiment was conducted with the same structure as the VR experiment and using auditory stimulus previously used to induce a defensive behavior detectable as a pupillary and behavioral response (Xiong et al., 2015; Wang et al., 2019; Hersman et al., 2020; Li et al., 2021). An initial period of habituation was followed by auditory stimulation using two tones (tone 1, 3 kHz; tone 2, 4 kHz; duration, 20 s; interstimulus interval, 120 s; Fig. 2A,B). We first set out to evaluate whether CNN can detect event-related pupil transients (i.e., ERTs) because of sensory stimulation in the VR. We averaged pupil size and running velocity during a 15 s temporal window centered on visual stimulation (Fig. 3C). We detected a significant pupillary dilation after the onset of the visual stimulus and no changes in evoked locomotion (pupil:  $p < 0.001$ , *post hoc* test; stimulus duration, 1.2–2.7 s; adjusted  $p$  values  $< 0.05$ , two-way repeated-measures ANOVA; velocity:  $p = 0.96$ , two-way repeated-measures ANOVA). This ERT is an orienting-related pupil response and a proxy of the arousal change because of stimulus detection (Wang and Munoz, 2015; Montes-Lourido et al., 2021). In the AS experiment, we also found an increase in pupil size, but dilation was associated with a significant increase in stimulus-induced locomotor activity (pupil:  $p < 0.001$ , *post hoc* test; stimulus duration, 1–10 s;

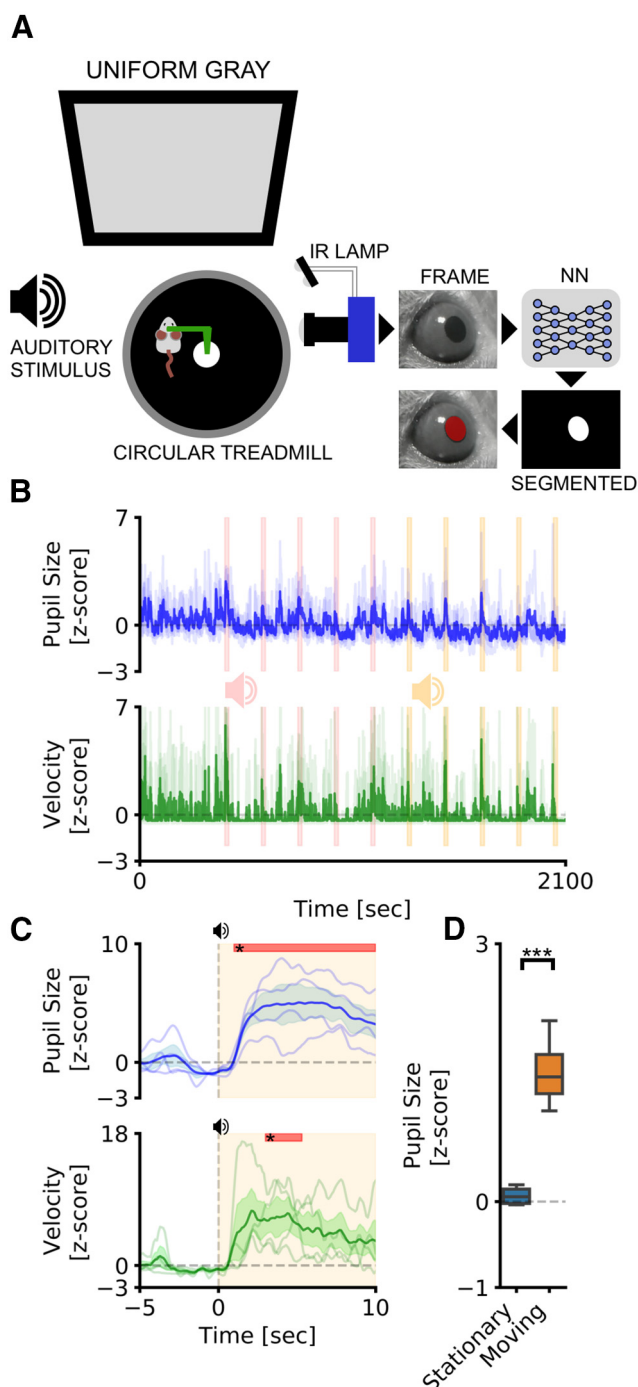


**Figure 2.** Pupillometry in head-fixed mice. **A**, Setup for head-fixed pupillometry in the awake mouse. The head of the mouse is fixed to a custom-made metal arm equipped with a 3D-printed circular treadmill to monitor running behavior. In the meantime, pupillometry is performed using CNN. **B**, The average fluctuations of pupillometry and velocity in all experimental mice. Dashed pink and yellow areas represent the onset and duration of auditory stimuli. Evoked peaks in both pupil size (blue line) and velocity (green line) are clearly noticeable during auditory stimulation. **C**, Average event-related transients for both pupil size and velocity. Colored areas represent stimulus onset and duration. Red areas in the top part of the plot represent statistically significant data points. **D**, Sensibility of the

adjusted  $p$  values  $< 0.05$ , two-way repeated-measures ANOVA; velocity:  $p > 0.01$ , *post hoc* test; stimulus duration, 3–5.3 s; adjusted  $p$  values  $< 0.05$ ; two-way repeated-measures ANOVA; Fig. 2C). Finally, we calculated pupil size during baseline periods before sensory stimulation both in the VR and the AS experiments. We found that during locomotion the pupil was significantly larger than in stationary periods both in the AS ( $p < 0.01$ , paired  $t$  test; Fig. 2D) and in the VR ( $p < 0.01$ , paired  $t$  test; Fig. 3D) experiments.

These results demonstrate that CNN pupillometry can detect the mouse locomotion-induced and stimulus-evoked pupillary changes and can be used to monitor behavioral state change during head fixation experiments.

### Web browser application to perform real-time pupillometry experiments

To greatly expand the use of our CNN-based pupillometer, we implemented the CNN in a web browser (MEYE; Fig. 4B), and we tested whether it could also be used in humans. To test this possibility, we designed a simple experiment aimed to measure PLR evoked by brief flashes of light on the human eye. The experiment included 10 flash events with an interstimulus interval of 5 s (Fig. 4C, dashed vertical lines). The results showed a clear light-induced modulation of pupil size in correspondence with each flash onset. Aligning and averaging all the traces along with the events, PLR can be quantified in both the raw trace (change from baseline,  $44.53 \pm 0.67\%$ ) and z-scored trace (SD from baseline,  $14.59 \pm 2.05$ ; Fig. 3D,E). To detect whether it is possible to measure cognitively driven pupil signals using the reliable MEYE tool, we performed pupillometry while participants executed an odd-ball task, a commonly used paradigm for cognitive and attentional measurement. This task is based on the principle by which pupil dilation is stronger in response to rare stimuli and can be used as a physiological marker for the detection of deviant stimuli (Liao et al., 2016). This experiment has been conducted by recording the same eye using both the MEYE tool and an EyeLink 1000 system. According to Google Scholar, the EyeLink 1000 system is one of the most used eye trackers in psychology, psychophysics, and neuroscience, with  $>17,000$  scientific publications mentioning this tool. During the oddball experiment, the subject was instructed to maintain fixation on a small dot presented in the center of the screen, pushing a button only when the Target stimulus appears on the screen and not responding to the Standard stimulus (Fig. 5A). Averaging and comparing the responses to Standard and Target gratings result in significantly stronger pupil dilation for the Target stimulus than the Standard stimulus, which is detected by both of the recording systems (MEYE:  $p < 0.001$ , paired

*continued*

system to detect locomotor-induced arousal fluctuations. Average pupil size is significantly affected by the behavioral states of the animal. During running epochs (Moving) the pupil is significantly more dilated than during the resting state (Stationary).  $***p > 0.001$ .

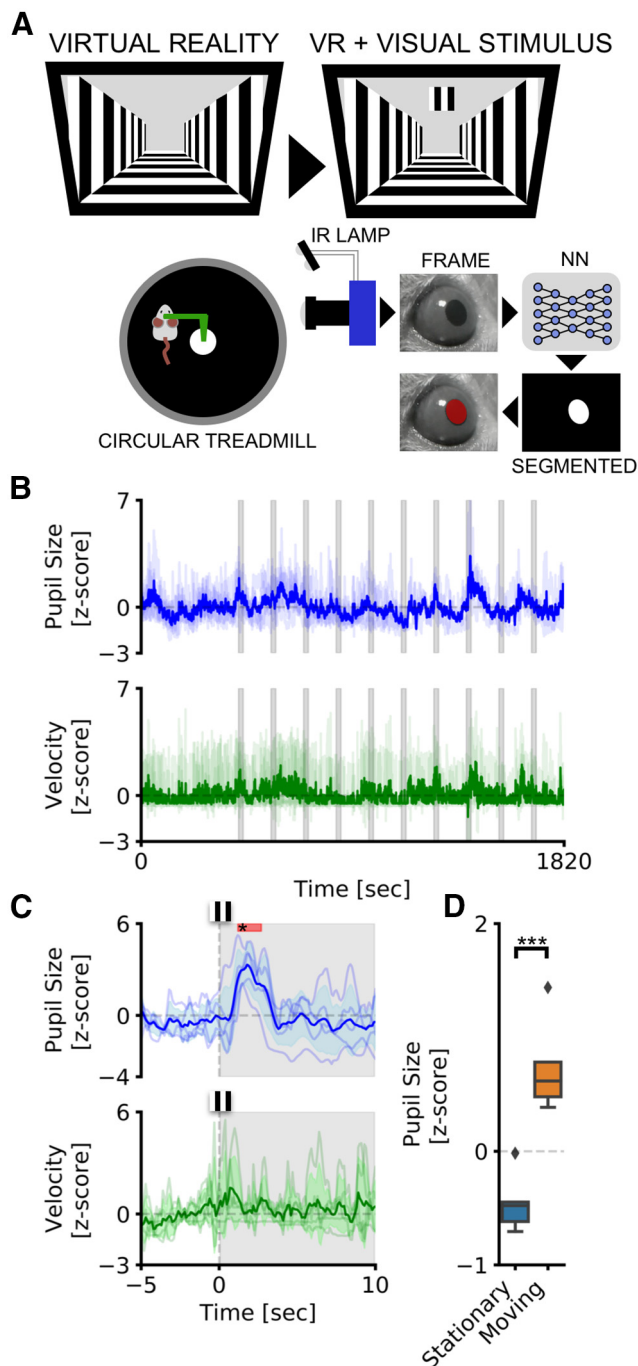


**Figure 3.** Pupillometry and VR in head-fixed mice. **A**, Setup for head-fixed pupillometry in VR in the awake mouse, showing the habituation phase (left), in which only the virtual corridor is shown, and the stimulation phase, in which a visual stimulus appears above the virtual corridor, in the binocular portion of the visual field. **B**, The average fluctuations of pupillometry and velocity in all experimental mice. Dashed gray areas represent the onset and duration of auditory stimuli. **C**, Average event-related transients for both pupil size and velocity. Colored areas represent stimulus onset and duration. Red areas in the top part of the plot represent statistically significant data points. **D**, Sensibility of the system to detect locomotor-induced arousal fluctuations. Average pupil size is significantly affected by the behavioral states of the animal. During running epochs (Moving), the pupil is significantly more dilated than during the resting state (Stationary).  $***p > 0.001$ .

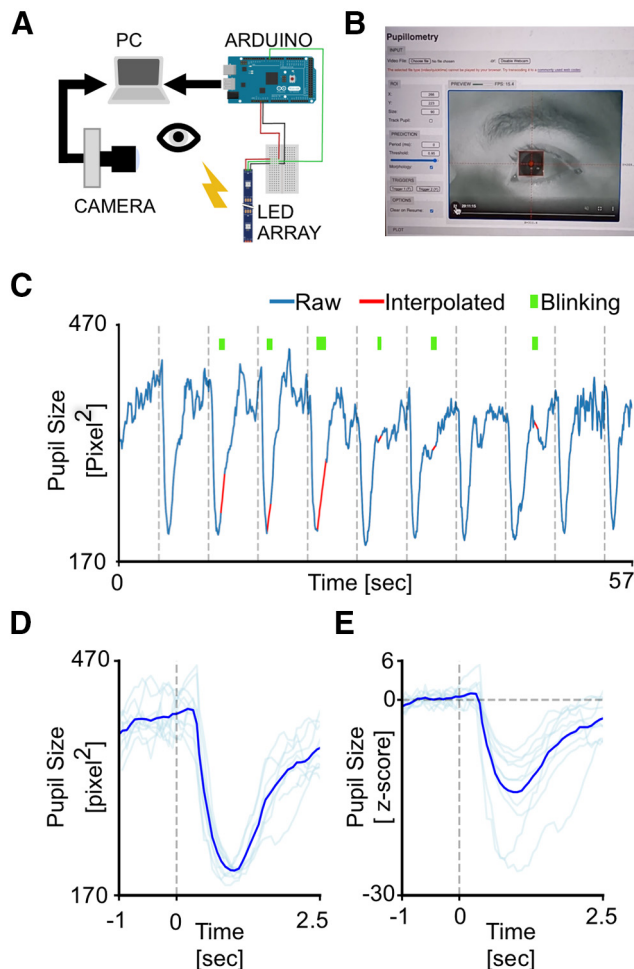


**Figure 4.** Web browser pupillometry experiment. **A**, Experimental setup for running the PLR stimulation and in the meantime performing pupillometric recordings. The PC is connected to the Internet by running an instance of the MEYE tool in the web browser. A USB camera, equipped with an IR light source, is focused on the eye of the subject. The photic stimulus is delivered using an LED array driven by an Arduino Due microcontroller board. The Arduino Due board is connected to the PC, emulating a keyboard and sending keystroke stimulus triggers to the MEYE tool. **B**, A picture of MEYE GUI. The subject during the recording is visualized as a streaming video. An ROI is used to locate the eye, and a preview of the estimation of the pupil is superimposed on the image of the subject. The GUI allows to set different parameters of postprocessing (map thresholding and refinement via mathematical morphology). **C**, Raw trace of the experiment (blue). Dashed lines locate the onset of flash stimuli. The green rectangles locate the onset and duration of blinks. The samples corresponding to blinks are removed and linearly interpolated (in red). **D**, Average event-related transient to flash stimulation in raw values. After the onset of the stimulus (dashed line), a strong constriction of the pupil is observed (44.53%). **E**, The z-score of the average event-related transient seen in **D**. The average nadir amplitude is 14.59 SDs from baseline.

*t* test; EyeLink:  $p < 0.001$ , paired *t* test; Fig. 5B,C). No differences have been found for the responses evoked by the Target stimulus between the MEYE tool and the EyeLink system ( $p = 0.327$ , paired *t* test; Fig. 4B, inset).



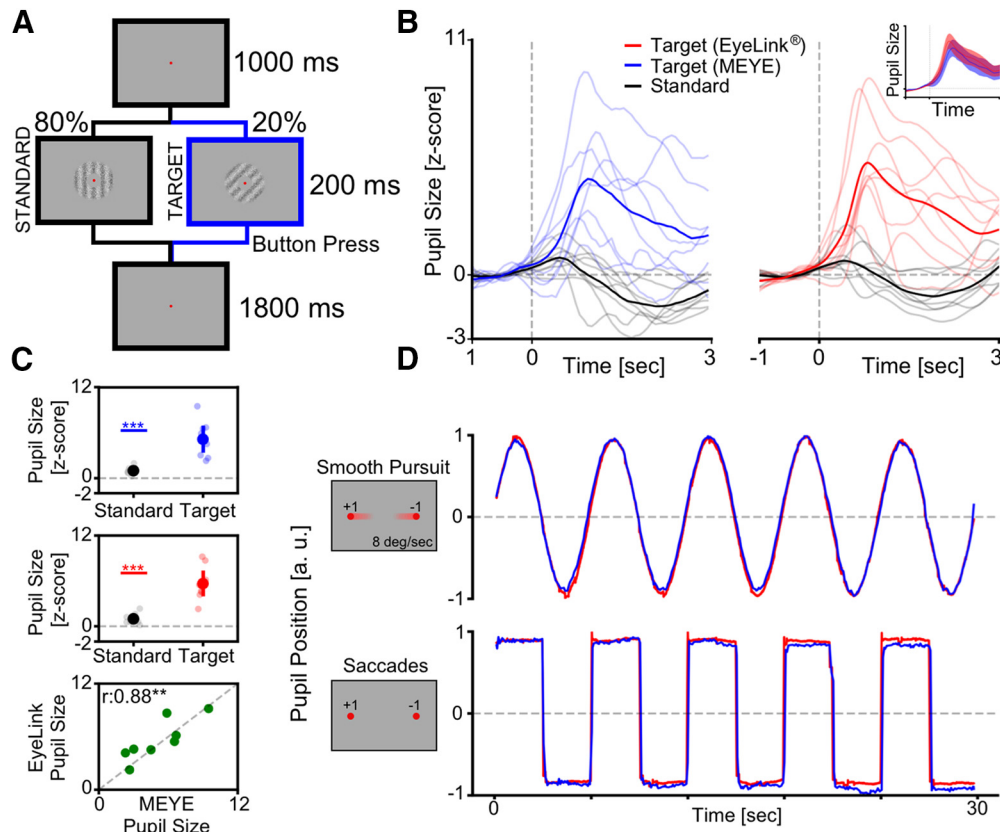


**Figure 5.** Cognitively driven pupillary changes. **A**, Visual oddball procedure. The participant is instructed to fixate a small red dot placed at the center of the screen and to push a button only when the Target visual stimulus appears. **B**, Average pupil waveforms. Average pupil response to Standard and Target stimuli for both the MEYE tool (blue, left) and the EyeLink system (red, right). The inset represents comparison between the evoked response to the Target stimulus in both setups. **C**, Average pupil response. Difference between the Standard and Target stimuli recording using the MEYE tool (top) and the EyeLink system (middle). The bottom graph represents the correlation between MEYE and EyeLink data. **D**, Eye movement data. Comparison between the MEYE tool (blue) and EyeLink system (red) during smooth pursuit task (top) and saccades (bottom).

Moreover, the single-subject pupillary evoked amplitudes show a significant positive correlation between the two techniques ( $\rho = 0.88$ ,  $p = 0.01$ , Spearman correlation) with  $>75\%$  of the variability explained by the linear model. Pupil size is known to covary with eye position in video-based measurements (Hayes and Petrov, 2016), producing foreshortening of the pupillary image because the camera is fixed but the eye rotates. To overcome this issue, there are several possible solutions, as follows: the simplest one requires constant fixation throughout each trial, but, if this requirement cannot be satisfied (e.g., in sentence reading), the position of the pupil at each sample can be used to correct and mitigate the estimation error. Thus, we decided to quantify the agreement between positional outputs provided by MEYE and EyeLink for horizontal eye movements. We designed the following two tasks: in the first task, a dot smoothly traveled horizontally on the screen from left to right and vice versa at a velocity of  $8^\circ/\text{s}$  and spanning  $20^\circ$ , producing slow and smooth pursuit eye movements. In the other experiment, a dot jumped every 5 s from one position to the other (spanning  $20^\circ$ ), producing large, fast, and abrupt saccades. Results (Fig. 4D) show that smooth pursuit movements generate a sinusoidal change of position

with a good agreement between both systems (MAE, 0.04). The second task, inducing saccades, produces a slightly larger error (MAE, 0.073). This error is mainly because of the much lower sampling rate of MEYE (MEYE, 15 fps; EyeLink, 1000 fps). This means that even if MEYE provides the exact positional information for each sample, it has a lower performance in adequately describing fast eye movements, such as saccades. Thus, MEYE provides the data required for *post hoc* correction of pupil measures, although it should be used with caution for measuring saccades.

### Web browser application to perform pupillometry on videos

MEYE can also be used as an offline tool to analyze pupillometry videos in various file formats, depending on the video codec installed in the web browser. To demonstrate the feasibility of performing pupillometry on videos captured in a variety of situations and in both mice and humans, we sampled three videos with a duration of 40 s from different experiments carried in our laboratory. Each video can be loaded as a demonstration in the web app to reproduce the same plots seen in Figure 6. Three

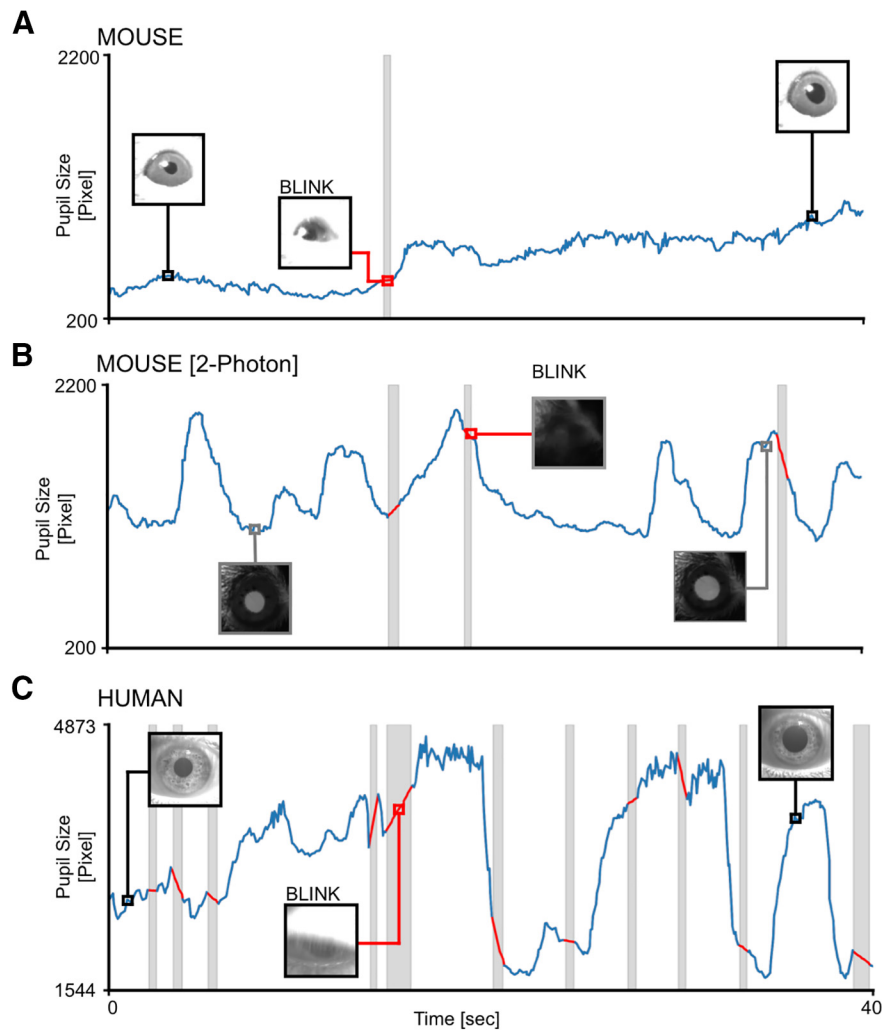


**Figure 6.** Offline movies analysis. **A**, Awake head-fixed mouse running on a treadmill, recorded for 40 s. The gray area represents a blink, and the trace of the blink is removed and linearly interpolated (red line). **B**, Awake mouse during two-photon calcium imaging. Here a brighter pupil is clearly visible with respect to **A**. Blinking epochs are removed and linearly interpolated. **C**, Pupillometry performed on a human subject, with a higher blinking rate with respect to mice. In all figures, the inset images represent the ROIs.

conditions were analyzed. The first condition can be found by pressing the “Mouse” button in the DEMO section of the graphical UI (GUI). It depicts a head-fixed mouse running on a circular treadmill under IR illumination and watching a uniform gray screen at  $10 \text{ cd/m}^2$  (Fig. 6A). The second is a mouse under a two-photon microscope (button “2P mouse”), walking on a cylindrical treadmill and showing clear dilation events because of locomotion (Fig. 6B). The third is found by pressing the button “Human,” starting 40 s of footage of a human subject wearing VR goggles projecting a uniform gray at  $15 \text{ cd/m}^2$  (Fig. 6C). These results show that offline pupillometry can be performed in various conditions and in both mice and humans.

## Discussion

In this work, we demonstrated that MEYE is a sensitive tool that can be used to study pupil dynamics in both humans and mice. Furthermore, by providing eye position,

MEYE allows *post hoc* control of the possible effects of eye movements on pupil measures (Hayes and Petrov, 2016). MEYE can detect both locomotion-induced and stimulus-evoked pupil changes with a peak latency of 1 s in a variety of conditions: mice with black pupils in normal illumination conditions; and mice with bright pupils resulting from laser infrared illumination. This flexibility allows the use of MEYE in combination with two-photon, wide-field imaging, and electrophysiological techniques widely adopted in awake or anesthetized mice. Furthermore, MEYE can be used to design stand-alone experiments using cost-effective hardware with performance comparable with that of state-of-the-art commercial software. In this experiment, we used a USB webcam with a varifocal objective that allows focal adjustment concentrated on the eye. The cost of the imaging equipment is  $<50\text{€}$  (Tables 2, 3) and requires no knowledge of coding to set up. The flashing stimulus apparatus requires a basic understanding of Arduino boards and can be assembled at a price of  $<50\text{€}$ . The overall cost of the apparatus is

**Table 2: Hardware for PLR**

Part no.	Description	Quantity	Price (€)	Store	Manufacturer
Walfront5k3psmv97x	USB webcam	1	33.48	Amazon	Walfront
149129	Varifocal M12 lens	1	12.03	Amazon	Sodial
A000062	Microcontroller Arduino Due	1	35	Arduino store	Arduino
1312	4 NeoPixel RGB LEDs	1	6.53	Adafruit	Adafruit
Total amount			87.04		

**Table 3: Statistical table**

Figure	Type of test	Statistical data
Figure 1	No statistical tests	
Figure 2C	Two-way repeated-measures ANOVA	Pupil: $F = 10.56, p < 0.001, \eta^2 = 0.43$ Velocity: $F = 1.47, p < 0.01, \eta^2 = 0.2$
Figure 2D	Parametric paired $t$ test	$T = -8.4395, p < 0.01, BF_{10} = 14.1$
Figure 3C	Two-way repeated-measures ANOVA	Pupil: $F = 7.42, p < 0.001, \eta^2 = 0.42$ Velocity: $F = 0.75, p < 0.96, \eta^2 = 0.1$
Figure 3D	Parametric paired $t$ test	$T = -11.1, p < 0.001, BF_{10} = 77.5$
Figure 5C1	Parametric paired $t$ test	$T = -4.64, p < 0.001, BF_{10} = 62.9$
Figure 5C2	Parametric paired $t$ test	$T = -5.41, p < 0.001, BF_{10} = 204.03$
Figure 5C3	Spearman correlation	$r = 0.9; 95\% \text{ CI} = [0.46, 0.98], r^2 = 0.78, p < 0.01, \text{power} = 0.9$
Figure 6	No statistical tests	

BF, Bayes factor.

<100€. Our code can be used in two different ways, to satisfy many needs. One way relies on the stand-alone web browser tool, which allows running MEYE on almost any device, from scientific workstations to notebooks or even smartphones. The other way uses a dedicated Python script running the CNN locally on a workstation. This latter case is suited for experiments with specific requirements, like high and stable frame rate or online processing of pupil size in which on-the-fly pupil computer interaction is required.

### Comparison with other methods

Valid open-source and commercial alternatives exist, but most of them are dedicated to gazing tracking and/or pupillometry. Commercial options are costly (<https://tobii.com>, <https://sr-research.com>, <https://neuroptics.com>), whereas open-source code requires programming knowledge and most open-source alternatives are explicitly dedicated to one species (Yiu et al., 2019; Privitera et al., 2020). One study (Privitera et al., 2020) assessed pupil dilation in mice through DeepLabCut (Mathis et al., 2018), a technique for 3D markerless pose estimation based on transfer learning. This approach, albeit powerful, is conceptually different since it is trained on user-defined key points instead

of on using the entire pupil to perform semantic segmentation. The former technique is more suited to track and locate arbitrary objects on an image, while the latter technique is focused on a more precise quantification of even small changes of the object area since pixelwise segmentation masks are refined iteratively using local and global contexts.

We compared our architecture with the first stage of DeepLabCut, which implements an image segmentation task (leaving out keypoint extraction), which is in common with our pipeline.

For a fair comparison, we trained the image segmentation networks used in DeepLabCut on our dataset. Table 4 shows that our architecture can achieve a higher number of frames per second and a superior segmentation performance (higher dice coefficient) with respect to the DeepLabCut models.

### Possible preclinical and clinical applications

The possible contribution of the web app technology resides in its portability: no software needs to be manually installed, and configuration is minimal. Only a clear IR image of the subject's eye is required. The performances of the tool are dependent on the host computer, but it runs at >10 fps in most of the machines tested. This

**Table 4: Comparison among CNN models**

CNN model	Train/test set	mDice	FPS (Web <sup>a</sup> )	FPS (Keras <sup>b</sup> )	FLOPS	Parameters, $n$
mini-UNet	Human/mouse eyes	84.0%	23.2	45.2	0.2G	0.03 M
DeepLabv3+/ResNet-50	ImageNet + finetune on human/mouse eyes	80.1%	<1	28.7	14.1G	26.8 M
DeepLabv3+/Lite-MobileNet-V3-Small	ImageNet + fine-tune on human/mouse eyes	69.0%	18.8	34.8	0.3G	1.1 M

<sup>a</sup>Dell Laptop: Intel(R) Core(TM) i7-9750H CPU @ 2.60 GHz; Intel UHD graphics 630 GPU; TensorFlow.js; backend: WebGL Browser: Microsoft edge 90.0.818.56.

<sup>b</sup>Ubuntu PC: Intel(R) Core(TM) i9-9900K CPU @ 3.60 GHz; GeForce RTX 2080 Ti GPU; Python 3.6.9 + TensorFlow 2.4.1. FLOPS, Floating point Operations Per Second; G, gigaFLOPS; M, mefaFLOPS.

advantage is particularly useful for settings with limited resources and space or for educational purposes. Web browser-embedded pupillometry will also be crucial for human scientific research, and clinical and preventive medicine. It would also be a promising tool in the recently growing field of telemedicine, given its minimal setup that can run on an average notebook computer or even on a smartphone, and that it allows possible large-scale recruitment of subjects directly in their own homes. This greatly facilitates infant, psychiatric, and motor-impaired patients' compliance, particularly for longitudinal research designs. We also released an open-source database of eyes composed of >11,000 images in various settings: head-fixed mice (black pupil); head-fixed two-photon imaging mice (white pupil); and human eyes. This dataset will grow over time to introduce new species and new use cases to increase, update, and strengthen MEYE performance. An updated list of planned and executed developments of MEYE can be found in the "Future Development" section of the GitHub Wiki. The possible scenarios can be further expanded in the future, because of the dynamic nature of CNN. It can be updated from the source, providing instantaneous updates on each computer running an instance of the program. Our hope is to create a community that refines and consolidates pupillometric performances to produce a tool that can be applied in different environments.

## References

- Aggius-Vella E, Gori M, Animalì S, Campus C, Binda P (2020) Non-spatial skills differ in the front and rear peri-personal space. *Neuropsychologia* 147:107619.
- Aleman TS, Jacobson SG, Chico JD, Scott ML, Cheung AY, Windsor EAM, Furushima M, Michael Redmond T, Bennett J, Palczewski K, Cideciyan AV (2004) Impairment of the transient pupillary light reflex in *Rpe65*<sup>-/-</sup> mice and humans with leber congenital amaurosis. *Invest Ophthalmol Vis Sci* 45:1259–1271.
- Angulo-Chavira AQ, García O, Arias-Trejo N (2017) Pupil response and attention skills in Down syndrome. *Res Dev Disabil* 70:40–49.
- Artoni P, Piffer A, Vinci V, LeBlanc J, Nelson CA, Hensch TK, Fagioli M (2020) Deep learning of spontaneous arousal fluctuations detects early cholinergic defects across neurodevelopmental mouse models and patients. *Proc Natl Acad Sci U S A* 117:23298–23303.
- Azevedo-Santos IF, DeSantana JM (2018) Pain measurement techniques: spotlight on mechanically ventilated patients. *J Pain Res* 11:2969–2980.
- Beggiato M, Hartwich F, Krems J (2018) Using smartbands, pupillometry and body motion to detect discomfort in automated driving. *Front Hum Neurosci* 12:338.
- Binda P, Pereverzeva M, Murray SO (2013a) Attention to bright surfaces enhances the pupillary light reflex. *J Neurosci* 33:2199–2204.
- Binda P, Pereverzeva M, Murray SO (2013b) Pupil constrictions to photographs of the sun. *J Vis* 13(6):8, 1–9.
- Blaser E, Eglington L, Carter AS, Kaldy Z (2014) Pupillometry reveals a mechanism for the autism spectrum disorder (ASD) advantage in visual tasks. *Sci Rep* 4:4301.
- Brainard DH (1997) The Psychophysics Toolbox. *Spat Vis* 10:433–436.
- Burley DT, van Goozen SHM (2020) Pupil response to affective stimuli: a biomarker of early conduct problems in young children. *J Abnorm Child Psychol* 48:693–701.
- Charier D, Vogler M-C, Zantour D, Pichot V, Martins-Baltar A, Courbon M, Roche F, Vassal F, Molliex S (2019) Assessing pain in the postoperative period: analgesia Nociception Index™ versus pupillometry. *Br J Anaesth* 123:e322–e327.
- Chen L-C, Zhu Y, Papandreou G, Schroff F, Adam H (2018) Encoder-decoder with atrous separable convolution for semantic image segmentation. In: *Computer Vision - ECCV 2018 15th European Conference, Munich, Germany, September 8-14, 2018, Proceedings*. Cham, Switzerland: Springer International.
- Chougule PS, Najjar RP, Finkelstein MT, Kandiah N, Milea D (2019) Light-Induced Pupillary Responses in Alzheimer's Disease. *Front Neurol* 10:360.
- Connelly MA, Brown JT, Kearns GL, Anderson RA, St Peter SD, Neville KA (2014) Pupillometry: a non-invasive technique for pain assessment in paediatric patients. *Arch Dis Child* 99:1125–1131.
- El Ahmadieh TY, Bedros N, Stutzman SE, Nyancho D, Venkatachalam AM, MacAllister M, Ban VS, Dahdaleh NS, Aiyagari V, Figueroa S, White JA, Batjer HH, Bagley CA, Olson DM, Aoun SG (2021) Automated pupillometry as a triage and assessment tool in patients with traumatic brain injury. *World Neurosurg* 145:e163–e169.
- Frost S, Robinson L, Rowe CC, Ames D, Masters CL, Taddei K, Rainey-Smith SR, Martins RN, Kanagasalingam Y (2017) Evaluation of cholinergic deficiency in preclinical Alzheimer's disease using pupillometry. *J Ophthalmology* 2017:7935406.
- Gajardo AJ, Madariaga S, Maldonado PE (2019) Autonomic nervous system assessment by pupillary response as a potential biomarker for cardiovascular risk: a pilot study. *J Clin Neurosci* 59:41–46.
- Hayes TR, Petrov AA (2016) Mapping and correcting the influence of gaze position on pupil size measurements. *Behav Res Methods* 48:510–527.
- He K, Zhang X, Ren S, Sun J (2016) Identity mappings in deep residual networks. In: *Computer vision — ECCV 2016: 14th European Conference, Amsterdam, the Netherlands, October 11-14, 2016, Proceedings. Part VII*. Cham, Switzerland: Springer International.
- Hersman S, Allen D, Hashimoto M, Brito SI, Anthony TE (2020) Stimulus salience determines defensive behaviors elicited by aversively conditioned serial compound auditory stimuli. *Elife* 9:e53803.
- Howard A, Sandler M, Chen B, Wang W, Chen L-C, Tan M, Chu G, Vasudevan V, Zhu Y, Pang R, Adam H, Le Q (2019) Searching for MobileNetV3. In: *2019 IEEE/CVF international conference on computer vision (ICCV)*. Piscataway, NJ: IEEE.
- Iadanza E, Goretti F, Sorelli M, Melillo P, Pecchia L, Simonelli F, Gherardelli M (2020) Automatic detection of genetic diseases in pediatric age using pupillometry. *IEEE Access* 8:34949–34961.
- Krebs RM, Park HRP, Bombeck K, Boehler CN (2018) Modulation of locus coeruleus activity by novel oddball stimuli. *Brain Imaging Behav* 12:577–584.
- Lee CR, Margolis DJ (2016) Pupil dynamics reflect behavioral choice and learning in a Go/NoGo tactile decision-making task in mice. *Front Behav Neurosci* 10:200.
- Liao H-I, Yoneya M, Kidani S, Kashino M, Furukawa S (2016) Human pupillary dilation response to deviant auditory stimuli: effects of stimulus properties and voluntary attention. *Front Neurosci* 10:43.
- Li Z, Wei J-X, Zhang G-W, Huang JJ, Zingg B, Wang X, Tao HW, Zhang LI (2021) Corticostriatal control of defense behavior in mice induced by auditory looming cues. *Nat Commun* 12:1040.
- LoTempio S, Silcox J, Federmeier KD, Payne BR (2021) Inter- and intra-individual coupling between pupillary, electrophysiological, and behavioral responses in a visual oddball task. *Psychophysiology* 58:e13758.
- Mathis A, Mamidanna P, Cury KM, Abe T, Murthy VN, Mathis MW, Bethge M (2018) DeepLabCut: markerless pose estimation of user-defined body parts with deep learning. *Nat Neurosci* 21:1281–1289.
- Mathôt S, Melmi J-B, van der Linden L, Van der Stigchel S (2016) The mind-writing pupil: a human-computer interface based on decoding of covert attention through pupillometry. *PLoS One* 11:e0148805.
- McGinley MJ, Vinck M, Reimer J, Batista-Brito R, Zagha E, Cadwell CR, Tolias AS, Cardin JA, McCormick DA (2015) Waking state: rapid variations modulate neural and behavioral responses. *Neuron* 87:1143–1161.

- Montes-Lourido P, Kar M, Kumbam I, Sadagopan S (2021) Pupillometry as a reliable metric of auditory detection and discrimination across diverse stimulus paradigms in animal models. *Sci Rep* 11:3108.
- Nyström P, Gliğa T, Nilsson Jobs E, Gredebäck G, Charman T, Johnson MH, Bölte S, Falck-Ytter T (2018) Enhanced pupillary light reflex in infancy is associated with autism diagnosis in toddlerhood. *Nat Commun* 9:1678.
- Obinata H, Yokobori S, Shibata Y, Takiguchi T, Nakae R, Igarashi Y, Shigeta K, Matsumoto H, Aiyagari V, Olson DM, Yokota H (2020) Early automated infrared pupillometry is superior to auditory brainstem response in predicting neurological outcome after cardiac arrest. *Resuscitation* 154:77–84.
- Oh AJ, Amore G, Sultan W, Asanad S, Park JC, Romagnoli M, La Morgia C, Karanjia R, Harrington MG, Sadun AA (2019) Pupillometry evaluation of melanopsin retinal ganglion cell function and sleep-wake activity in pre-symptomatic Alzheimer's disease. *PLoS One* 14:e0226197.
- Oh AJ, Amore G, Sultan W, Asanad S, Park JC, Romagnoli M, La Morgia C, Karanjia R, Harrington MG, Sadun AA (2020) Correction: pupillometry evaluation of melanopsin retinal ganglion cell function and sleep-wake activity in pre-symptomatic Alzheimer's disease. *PLoS One* 15:e0230061.
- Olivia C, Josef S, Camille C, Christof K, Steven L, Wolfgang E (2013) The use of pupil dilation to communicate with locked-in syndrome patients. In: ACNS-2013 Australasian Cognitive Neuroscience Society Conference. Callaghan, Australia: Australasian Cognitive Neuroscience Society.
- Pelli DG (1997) The VideoToolbox software for visual psychophysics: transforming numbers into movies. *Spat Vis* 10:437–442.
- Ponzio F, Villalobos AEL, Mesin L, de'Sperati C, Roatta S (2019) A human-computer interface based on the "voluntary" pupil accommodative response. *Int J Hum Comput Stud* 126:53–63.
- Privitera M, Ferrari KD, von Ziegler LM, Sturman O, Duss SN, Floriou-Servou A, Germain P-L, Vermeiren Y, Wyss MT, De Deyn PP, Weber B, Bohacek J (2020) A complete pupillometry toolbox for real-time monitoring of locus coeruleus activity in rodents. *Nat Protoc* 15:2301–2320.
- Reimer J, McGinley MJ, Liu Y, Rodenkirch C, Wang Q, McCormick DA, Tolia AS (2016) Pupil fluctuations track rapid changes in adrenergic and cholinergic activity in cortex. *Nat Commun* 7:13289.
- Ronneberger O, Fischer P, Brox T (2015) U-Net: convolutional networks for biomedical image segmentation. In: Medical image computing and computer-assisted intervention – MICCAI 2015, pp 234–241. Cham, Switzerland: Springer International.
- Rorick-Kehn LM, Witcher JW, Lowe SL, Gonzales CR, Weller MA, Bell RL, Hart JC, Need AB, McKinzie JH, Statnick MA, Suico JG, McKinzie DL, Tauscher-Wisniewski S, Mitch CH, Stoltz RR, Wong CJ (2014) Determining pharmacological selectivity of the kappa opioid receptor antagonist LY2456302 using pupillometry as a translational biomarker in rat and human. *Int J Neuropsychopharmacol* 18:pyu036.
- Silasi G, Xiao D, Vanni MP, Chen ACN, Murphy TH (2016) Intact skull chronic windows for mesoscopic wide-field imaging in awake mice. *J Neurosci Methods* 267:141–149.
- Stoll J, Chatelle C, Carter O, Koch C, Laureys S, Einhäuser W (2013) Pupil responses allow communication in locked-in syndrome patients. *Curr Biol* 23:R647–R648.
- Vallat R (2018) Pingouin: statistics in Python. *J Open Source Softw* 3:1026.
- Wang C-A, Munoz DP (2015) A circuit for pupil orienting responses: implications for cognitive modulation of pupil size. *Curr Opin Neurobiol* 33:134–140.
- Wang H, Chen J, Xu X, Sun W-J, Chen X, Zhao F, Luo M-H, Liu C, Guo Y, Xie W, Zhong H, Bai T, Tian Y, Mao Y, Ye C, Tao W, Li J, Farzinpour Z, Li J, Zhou J-N, Wang K, He J, Chen L, Zhang Z (2019) Direct auditory cortical input to the lateral periaqueductal gray controls sound-driven defensive behavior. *PLoS Biol* 17:e3000417.
- Wierda SM, van Rijn H, Taatgen NA, Martens S (2012) Pupil dilation deconvolution reveals the dynamics of attention at high temporal resolution. *Proc Natl Acad Sci U S A* 109:8456–8460.
- Winston M, Zhou A, Rand CM, Dunne EC, Warner JJ, Volpe LJ, Pigneri BA, Simon D, Bielawiec T, Gordon SC, Vitez SF, Charnay A, Joza S, Kelly K, Panicker C, Rizvydeen S, Niewijk G, Coleman C, Scher BJ, Reed DW, et al (2020) Pupillometry measures of autonomic nervous system regulation with advancing age in a healthy pediatric cohort. *Clin Auton Res* 30:43–51.
- Xiong XR, Liang F, Zingg B, Ji X-Y, Ibrahim LA, Tao HW, Zhang LI (2015) Auditory cortex controls sound-driven innate defense behaviour through corticofugal projections to inferior colliculus. *Nat Commun* 6:7224.
- Yiu Y-H, Aboulatta M, Raiser T, Ophey L, Flanagan VL, Zu Eulenburg P, Ahmadi S-A (2019) DeepVOG: open-source pupil segmentation and gaze estimation in neuroscience using deep learning. *J Neurosci Methods* 324:108307.
- Zhuang J, Tang T, Ding Y, Tatikonda S, Dvornek N, Papademetris X, Duncan JS (2020) AdaBelief optimizer: adapting stepsizes by the belief in observed gradients. *arXiv: 2010.07468*.